Applied Catalysis B: Environmental 310 (2022) 121350

Contents lists available at ScienceDirect

Applied Catalysis B: Environmental

journal homepage: www.elsevier.com/locate/apcatb

Decoration of CdS nanowires with Ni_3S_4 nanoballs enhancing H_2 and H_2O_2 production under visible light

Yaru Wang, Jianjun Zhao, Wenqing Hou, Yiming Xu *

State Key Laboratory of Silicon Materials and Department of Chemistry, Zhejiang University, Hangzhou, China

ARTICLE INFO

Keywords:
Photocatalysis
Visible light
Hydrogen
Hydrogen peroxide
Cadmium sulfide
Nickel sulfide

ABSTRACT

Much work in the past four decades has focused on CdS as photocatalyst for water splitting. Recently, Ni_3S_4 has been reported to be more active than IrO_2 as an electrocatalyst for water oxidation. Herein we report a positive role of Ni_3S_4 in CdS photocatalysis. Reaction was conducted in aqueous suspension under a 420 nm light, either for proton reduction to H_2 in presence of Na_2S and Na_2SO_3, or for O_2 reduction to H_2O_2 without addition of any sacrifices. In both cases, Ni_3S_4 were nearly not active. After Ni_3S_4 loading, however, the rates of H_2 and H_2O_2 production on CdS increased by factors as much as 21 and 3, respectively. Furthermore, Ni_3S_4/CdS was more efficient than CdS for proton and O_2 reduction on a cathode, respectively, while Ni_3S_4/CdS was less efficient than CdS for the photoelectron accumulation on an electrode at open circuit potential. Based on the solid photoluminescence spectra and band edge potentials, a possible mechanism is proposed, involving the interfacial electron transfer from CdS to Ni_3S_4, followed by an increased surface reaction, for proton (oxygen) reduction on Ni_3S_4 sites, and for sulfide (water) oxidation on CdS sites, respectively.

1. Introduction

Environmental pollution and energy crisis have spurred the exploitation of clean and renewable energy sources [1,2]. As one of the most promising solutions for these problems, semiconductor photocatalysis has attracted much attention. It is a "green" technology for decomposing water, inactivating viruses, and eliminating organic pollutants under ambient conditions [3]. Hydrogen, a green and carbon-free energy source, is an ideal candidate for replacing fossil fuels [4]. On the other hand, hydrogen peroxide, a widely used chemicals, is also a potential alternative to conventional fuels, if it is produced via simple, clean and cheap approaches [5,6]. In the photocatalytic system, a water-based reaction is often used for the generation of H_2 and H_2O_2, only with sun light, water, and oxygen as the inputs [7–9].

Hitherto, various visible-light-active photocatalysts have been developed, including metal oxides (Cu_2O, Fe_2O_3, and WO_3) [10–12], metal sulfides (Cu_2S, CdS, and In_2S_3) [13–17], Bi-based materials (Bi_2WO_6, BiOBr, and BiOI) [18–20], and g-C_3N_4-based materials [21, 22]. Among them, much work has focused on CdS, because it not only has a good visible-light response, but also an appropriate band structure enabling both water reduction and oxidation [23]. In general, a semiconductor on the band gap excitation generates electrons and holes in the conduction and valence bands, respectively. However, most of the photogenerated charge carriers quickly recombine, without chemical reactions with sorbates [24]. Beside that, CdS also suffers from a corrosion and deactivation, due to sulfides being oxidized into a high valence sulfur species [25]. To increase the efficiency and stability of CdS photocatalysis, much effort has been made [26]. For example, a NiS-deposited CdS is more photoactive than CdS for H_2 production under visible light. This is due to α- or β-NiS mediating the electron transfer from CdS to protons [27–29], and/or due to p-type semiconductor NiS and n-type semiconductor CdS forming a p-n junction and hence improving the efficiency of charge separation through a Z-scheme [30,31]. It seems that the performance of NiS are influenced by its morphologies and crystal structures.

Recently, Wang and co-workers have reported that Ni_3S_4 is more active than NiS, Ni_2S_3, and NiS_2, respectively, for the electrochemical oxidation of water [32]. They ascribed it to the adsorption energy of water on Ni_3S_4 being larger than those on other three sulfides, and being also close to that on IrO_2, an excellent catalyst for water oxidation, even in semiconductor photocatalysis [33]. Meanwhile, Wan and coworkers have prepared a Ni^{3+}-rich porous Ni_3S_4 via a Ni substituted metal organic framework (Ni-MOF). Interestingly, this sulfide was much more active than IrO_2, for the electrochemical oxidation of water, mainly due

* Corresponding author.
E-mail address: xuym@zju.edu.cn (Y. Xu).

https://doi.org/10.1016/j.apcatb.2022.121350
Received 16 February 2022; Received in revised form 20 March 2022; Accepted 23 March 2022
Available online 26 March 2022

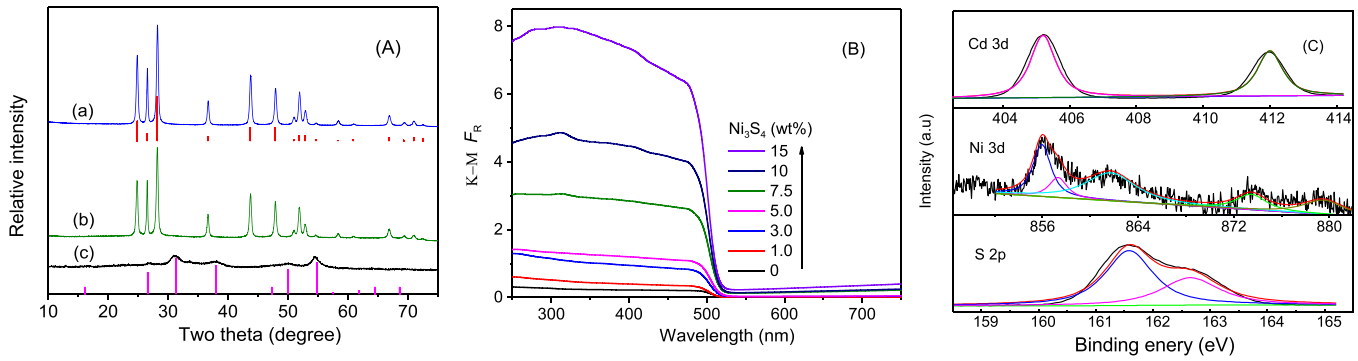

Fig. 1. (A) XRD patterns for (a) CdS, (b) NC-15, and (c) Ni_3S_4. The top and bottom column bars are the patterns for CdS (70–2553), and Ni_3S_4 (43–1469), respectively. (B) Absorption spectra for NC-*x*, where *x* is 0–15. (C) XPS spectra for NC-7.5.

to Ni^{3+} species facilitating OH^-/H_2O chemisorption and oxidation [34]. Then it is highly possible that Ni_3S_4 also plays an important role in a semiconductor photocatalysis, which is yet to be explored.

In this work, we report a positive effect of Ni_3S_4 on the photocatalytic reaction of CdS in aqueous solution under visible light. This was observed not only for proton reduction to H_2 in presence of Na_2S and Na_2SO_3 as hole sacrifices, but also for O_2 reduction to H_2O_2 without addition of any sacrifices. The composite materials were prepared simply by grinding CdS nanowires with Ni_3S_4 nanoballs, without further treatment, so that any changed reaction is surely due to the effect of Ni_3S_4. To understand the role of Ni_3S_4, several experiment were conducted, including the effect of Ni_3S_4 loading, the catalyst stability, and the electrochemical measurement for proton and O_2 reaction. Furthermore, a possible mechanism responsible for the observed effect of Ni_3S_4 is discussed, in terms of both thermodynamics and kinetics.

2. Experimental section

2.1. Materials

Nickel perchlorate, horseradish peroxide (POD), and N,N-diethyl-*p*-phenylenediamine (DPD) were purchased from Sigma-Aldrich, and others from Shanghai Chemicals, including $Cd(NO_3)_2$, ethylenediamine, urea, thiourea, Na_2S, and Na_2SO_3. All of the chemicals in analytical grade were used without any further purification.

2.2. Preparation of photocatalysts

2.2.1. Preparation of CdS Nanowires

The CdS nanowires were synthesized by a solvothermal method. Typically, 6.41 g $Cd(NO_3)_2.4\ H_2O$ and 4.74 g of thiourea were added into a dried Teflon-lined autoclave with a capacity of 200 mL. Afterwards, 100 mL of ethylenediamine was injected, and the autoclave was sealed and heated at 180 °C for 3 days. After cooling to room temperature, the yellow precipitates were collected, washed carefully with distilled water and anhydrous ethanol for 5 times, and finally dried at 60 °C in a vacuum oven.

2.2.2. Preparation of rose-like Ni_3S_4 microstructure

First, $Ni(OH)_2$ precursor was prepared by dissolving 0.33 g $Ni(ClO_4)_2.6\ H_2O$ and 0.36 g urea in 90 mL water, followed by stirring for 1 h, and heating at 130 °C for 4 h in a 150 mL Teflon-lined autoclave. After cooling to room temperature, the green powder was collected by centrifugation, and dried at 60 °C in a vacuum oven. Second, the precursor was mixed with 6.6 g $Na_2S{\cdot}9\ H_2O$ in 90 mL water, and the mixture was placed in an autoclave and heated at 90 °C for 9 h. After cooling down to room temperature, the black powder was washed with water and ethanol several times, followed by drying at 60 °C for 12 h in a vacuum oven.

2.2.3. Preparation of Ni_3S_4/CdS

The above CdS and Ni_3S_4 at different ratios were mixed in an agate mortar. The resulting solid was denoted as NC-x, where x presents the calculated weight percent of Ni_3S_4. For examples, NC-3.0 represents the solid containing 3 wt% Ni_3S_4.

2.3. Characterization of photocatalysts

X-ray diffraction (XRD) patterns were recorded on D/max-2550/PC diffractometer (Rigaku). Scanning electron microscope (SEM) was performed on a SU-8010 (Hitachi). High resolution TEM (HRTEM) image was obtained with a Tecnai G2 electron microscope (FEI, Netherlands). Adsorption−desorption isotherm of N_2 on solid was measured at 77 K on a Micromeritics ASAP2020 apparatus. Diffuse reflectance spectra were recorded on a Varian Carry 500 ($BaSO_4$ as a reference), and the reference (R) was transformed to Kubella−Munk unit, $F_R = (1\text{-}R)^2/2\ R$. Photoluminescence (PL) spectra were recorded on a Shimadzu F-2500 spectrophotometer (excitation at 338 nm). X-ray photoelectron spectra (XPS) were recorded on a Kratos AXIS Ultra DLD spectrometer, and calibrated with C 1 s at 284.8 eV.

2.4. Photocatalytic activity test

2.4.1. Production and detection of H_2

Reaction was carried out in an aqueous suspension (50 mL) containing 25 mg catalyst, 0.35 M Na_2S, and 0.25 M Na_2SO_3. First, the suspension was first purged with N_2 for 30 min, so as to remove the dissolved oxygen. Then the reactor was closed, and irradiated with four 3 W LED lamps ((420 nm). The amount of H_2 evolved in gas phase was determined by GC (gas chromatography) on an Agilent 7820 A, equipped with a thermal conductivity detector.

Apparent quantum yield (AQY) for H_2 production was measured under the same conditions as described above. The light intensity reaching the reactor external surface was measured with a UV-A radiometer (Beijing Shuda Technology Co., Ltd). AQY is defined as $2n_H/n_p$, where n_H is the number of H_2 molecules evolved in gas phase, and n_p is the number of incident photons. The latter (n_p) is calculated from $E_p/h\nu = IAt/h\nu$, in which E_p is the total energy of incident photons (J), h is plank constant (J/s), υ is light frequency (Hz), I is light intensity (W/m^2), A is irradiation area (m^2), and t is irradiation time (s) [35].

2.4.2. Production and detection of H_2O_2

Unless stated otherwise, reaction was carried out at 25 °C on a photochemical apparatus (Nanjing XuJiang Power Plant, China) under fixed initial conditions (25 mg catalyst, and 50 mL H_2O). The suspension was stirred in the dark for 30 min, and then irradiated with a 400 W metal halide lamp equipped with a 420 nm cut-off filter. The light intensity reaching the external surface of reactor was 4.0 mW/cm^2. At given intervals, 4.0 mL of the suspension was withdrawn, and filtered

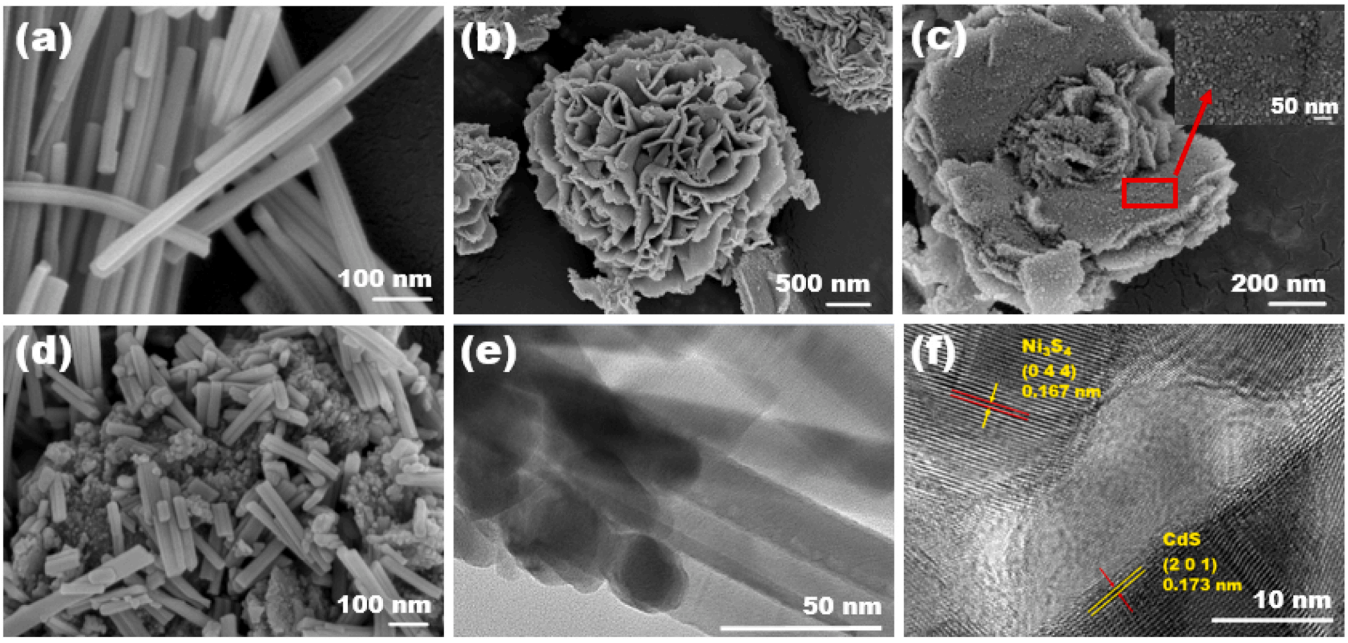

Fig. 2. SEM images for (a) CdS, (b, c) Ni_3S_4, (d) NC-7.5. (e, f) HRTEM images for NC-7.5.

through a 0.22 μm membrane. The filtrate was immediately analyzed for H_2O_2, through a POD-catalyzed oxidation of DPD [36]. The solution absorbance at 553 nm was recorded on an Agilent 8453 UV–vis spectrophotometer.

2.5. (Photo)electrochemical measurements

Experiment was carried out on a CHI660E Electrochemical Station (Chenhua, Shanghai), using a platinum gauze as counter electrode, and a Ag/AgCl electrode as reference electrode. A working electrode was prepared by coating a fluorine-doped tin oxide glass with 30 μL slurry (10 mg catalyst, 1.5 mL N, N-dimethylformamide, and 60 μL Nafion perfluorinated resin), followed by drying in an oven at 60 °C overnight. The working electrode was illuminated with a 500 W Xe lamp (10.0 mW/cm^2) from the electrode/electrolyte side through a quartz window. Electrolyte was 0.5 M $NaClO_4$, and scanning rate was 10 mV/s. Electrochemical impedance spectroscopy (EIS) was conducted at 100 kHz − 1 Hz in an at open-circuit mode. Mott-Schottky plot was obtained by measuring the capacitance at 1 kHz as a function of potential.

3. Results and discussion

3.1. Solids characterization

Solid crystal structure was examined by XRD (Fig. 1A). For CdS, the diffractions at 24.8°, 26.5°, 28.2°, 36.7°, 43.7°, 51.9°, and 66.8° corresponded to the (100), (002), (101), (110), (103), (112) and (203) facets for hexagonal CdS, respectively. For Ni_3S_4, the peaks centered at 25.6°, 31.3°, 38.0°, 50.0°, and 54.8° were indexed to the (022), (113), (004), (115) and (044) facet for cubic Ni_3S_4, respectively. But Ni_3S_4 was poorly crystalized, as compared with CdS. After CdS was grinded with 7.5 wt% Ni_3S_4, the solid (denoted as NC-7.5) showed a pattern similar to that of CdS. All NC-x (x = 0–15 wt%) had similar cell parameters and crystallite size for CdS (Table S1 and Fig. S1). But no Ni_3S_4 was observed, due to its poor crystallinity and low content.

Fig. 1B shows the solid absorption spectra. CdS absorbed light at wavelengths up to 520 nm, while Ni_3S_4 had a wide band at 200–800 nm (Fig. S2). For NC-x, the spectrum shifted upward, as the Ni_3S_4 content was increased. This is due to Ni_3S_4 having a larger absorbance than CdS at given wavelength. Through a Tauc plot, the direct band gap energy (E_g) was estimated, which was 2.38 eV for CdS, 1.74 eV for Ni_3S_4, and 2.39 eV for all NC-x (Fig. S2). Fig. 1C shows the XPS spectra for NC-7.5. The binding energies at 405.2 eV (Cd $3d_{5/2}$), 412.0 eV (Cd $3d_{3/2}$), 161.6 eV (S $2p_{3/2}$), and 162.7 eV (S $2p_{1/2}$) matched those reported for Cd^{2+} and S^{2-}, respectively [27–31]. In the high resolution spectrum of Ni $2p_{3/2}$, the signals due to Ni^{2+} at 855.90 eV and Ni^{3+} at 857.30 eV were both observed [34]. According to the integrated peak area, the mole ratio of Ni^{3+} to Ni^{2+} was approximately 0.39, which was higher than that for NiS [27–31], but lower than that for a Ni-MOF-derived Ni_3S_4 [34]. Except those species, no signals due to polysulfide and sulfonate at 164–169 eV were observed [34,37].

Fig. 2 shows the solid photographs. In the SEM images, CdS was nanowires (20–40 nm in diameter, and 2 −4 μm in length), while Ni_3S_4 was rose-like particles, and its subunit sheets consisted of many tiny balls (5–10 nm in diameter). For NC-7.5, there were small particles (Ni_3S_4) around large nanowires (CdS). A HRTEM image revealed that CdS and Ni_3S_4 had a close contact. The adjacent lattice fringes due to (201) CdS at 0.173 nm and (203) CdS at 0.139 nm, and due to (044)

Table 1
Physical parameters and photoreaction data for different samples[a].

Samples	A_{sp} (m^2/g)	V_p (cm^3/g)	d_p (nm)	n_{H2h} (μmol)	n_{H2h}/A_{sp} (μmol/m^2)	AQY (%)
CdS	17.47	0.147	18.12	21.7	49.7	0.43
NC-1.0	18.67 (17.30)	0.149 (0.146)	19.03	210.4	450.7	4.17
NC-3.0	18.76 (16.96)	0.167 (0.143)	18.17	343.8	733.1	6.81
NC-5.0	19.27 (16.63)	0.153 (0.140)	17.73	395.3	820.6	7.84
NC-7.5	20.37 (16.29)	0.156 (0.137)	17.05	450.1	883.9	8.92
NC-10	20.69 (15.78)	0.168 (0.133)	17.07	397.1	767.8	7.87
NC-15	21.61 (14.94)	0.151 (0.126)	16.40	374.4	693.0	7.42
Ni_3S_4	0.58	0.009	30.77	0	–	–

[a] A_{sp}, surface area; V_p, total pore volume; d_p, average pore size; n_{H2h}, the amount of H_2 produced at 2 h. The bracket data are the values calculated from individuals; *AQY*, apparent quantum yield for H_2 production.

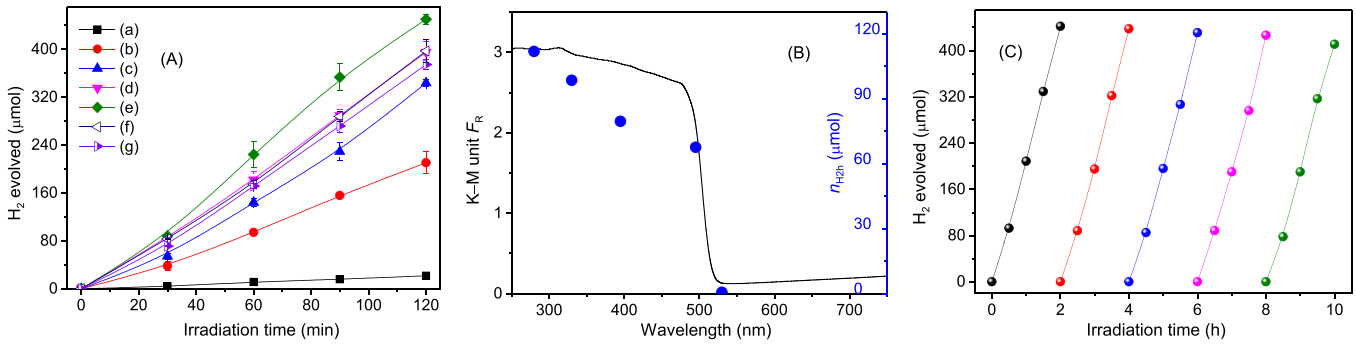

Fig. 3. (A) Photocatalytic evolution of H_2 under a 420 nm LED for (a) CdS, (b) NC-1.0, (c) NC-3.0 (d) NC-5.0, (e) NC-7.5, (f) NC-7.5, and (g) NC-15. (B) Amount of H_2 evolved at 2 h (n_{H2h}) for NC-7.5 under a Xenon lamp, cut-off at different wavelengths. Experiment was conducted in an aqueous solution of Na_2S/Na_2SO_3. (C) Repeat production of H_2 under a 420 nm LED. After each run, the catalyst was collected, and re-dispersed into a new solution of Na_2S/Na_2SO_3. Then the suspension was purged with N_2 for 30 min, followed by visible light illumination.

Ni_3S_4 at 0.167 nm were all observed (Fig. S3). Furthermore, an elemental mapping showed that all elements (S, Cd, and Ni) homogeneously distributed over NC-7.5.

Solid porosity was studied by N_2 adsorption and desorption isotherm (Fig. S1). For all Cd-containing samples, the isotherms were Type I, with a definite loop at high relative pressure. This is indicative of the micropores being present in those samples. Table 1 lists the solid surface area (A_{sp}), total pore volume (V_p), and average pore diameter (d_p). By comparison to CdS, Ni_3S_4 had a lower A_{sp}, a smaller V_p, and a larger d_p, respectively. After CdS and Ni_3S_4 were mixed, however, the NC-x (x = 1.0–15) had a A_{sp} and V_p value not only larger than that for CdS, respectively, but also larger than the sum of the A_{sp} values calculated from neat individuals, respectively. Meanwhile, most of the d_p values were smaller than those of CdS and Ni_3S_4, respectively. These observations indicate that during the grinding process, the CdS and Ni_3S_4 particles scrape each other, reducing the aggregate size, and building up a new microporous system. As a result, the solid surface area and pore volume are increased, respectively.

3.2. Photocatalytic H_2 production and stability test

Reactions were carried out in a N_2-pre-saturated aqueous solution containing 0.35 M Na_2S and 0.25 M Na_2SO_3. Fig. 3A shows the time profiles for H_2 production, measured under a 420 nm LED lamp. As the irradiation time increased, the amount of H_2 evolved in gas phase increased nonlinearly. To compare the relative catalyst activity, the amount of H_2 obtained at 2 h (n_{H2h}) was selected, and the results are shown in Table 1. We see that n_{H2h} greatly varies with the weight percent (x) of Ni_3S_4 in the samples. Because the catalysts have different surface area, the n_{H2h} is tentatively normalized to A_{sp}. In this case, NC-7.5 is also the most active among NC-x. In terms of the n_{H2h} and n_{H2h}/A_{sp}, the 7.5% Ni_3S_4 loaded CdS is more active than CdS by factors of approximately 20.7 and 16.5, respectively. Control experiment with Ni_3S_4 showed a negligible production of H_2 even at 3 h. Then the increased n_{H2h} or n_{H2h}/A_{sp} with x is indicative of Ni_3S_4 being involved in the photocatalytic process. After a maximum, the decreased n_{H2h} or n_{H2h}/A_{sp} with x is probably due to excess Ni_3S_4 absorbing visible light, reducing the number of photons reaching CdS, and hence slowing down the CdS-photocatalyzed formation of H_2.

The AQY for H_2 production was also measured under a 420 nm LED lamp. All NC-x samples had an AQY value larger than that measured for CdS (Table 1). Note that the AQY values is useful only as a reference, because the actual number of photons absorbed by a photocatalyst may change from one to another. Furthermore, the present NC-7.5 is also superior to several NiS-containing CdS samples (NiS/CdS) reported (Table S3). This is done in terms of the R_H/R_{H0}, where R_H and R_{H0} are the rates of H_2 production obtained for NiS/CdS and CdS, respectively. In general, the rate of H_2 production is dependent of many factors, including the light source and hole scavenger. Therefore, such comparison is used only as a reference.

Fig. 3B shows the production of H_2 on NC-7.5. measured under a Xenon lamp, cut-off at different wavelengths. At a shorter wavelength, the n_{H2h} was larger. Such the wavelength-dependent n_{H2h} well matched the absorption spectrum of NC-7.5. At 530 nm, the amount of H_2 produced at 2 h was negligible. At this wavelength, the absorbance of Ni_3S_4 was much larger than that of CdS. This is indicative of H_2 production resulting from CdS photocatalysis.

Fig. 3C shows the 5-repeated production of H_2 for 10 h. For each run, the conditions were fixed. After each run, the catalyst was centrifuged, and re-dispersed into a fresh solution of Na_2S and Na_2SO_3, followed by N_2 purging for 30 min and light irradiation for 2 h. From the first run to the fifth, the rate of H_2 production slightly decreased. The corresponding

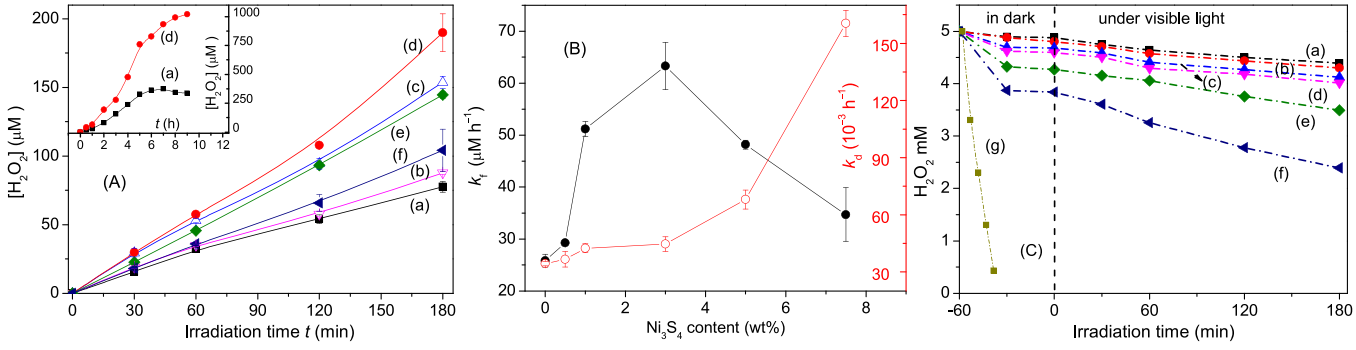

Fig. 4. (A) Photocatalytic production of H_2O_2 in aqueous phase, and (B) the corresponding rate constants for H_2O_2 formation (k_f) and decomposition (k_d). (C) Dark adsorption and photodecomposition of 5.0 mM H_2O_2. Samples were (a) CdS, (b) NC-0.5, (c) NC-1.0, (d) NC-3.0, (e) NC-5.0, (f) NC-7.5, and (g) Ni_3S_4. All experiments were carried out in an air-exposed aqueous solution without addition of sacrificial reagents.

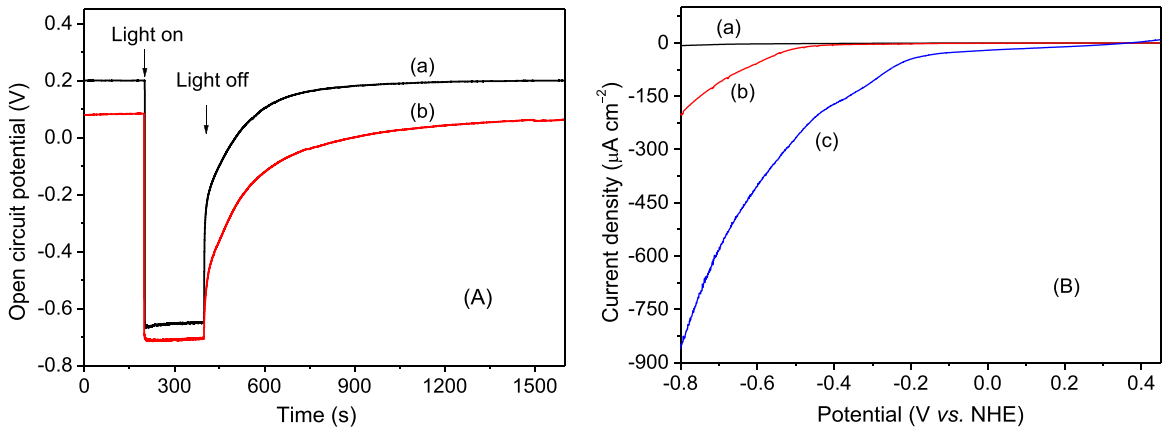

Fig. 5. (A) Open circuit potentials (OCP) test, and (B) proton reduction the dark, for a film electrode of (a) CdS, (b) NC-7.5, and (c) Ni_3S_4, measured in 0.5 M $NaClO_4$ under N_2.

n_{H2h} were 442, 438, 431, 427, and 411 μmol, respectively. To check the catalyst stability, the irradiated catalyst was collected, dried, and analyzed by XRD and XPS. After 10 h photoreaction, no significant change was observed, either in the solid crystal structure, or in the element chemical states (Fig. S4 and Table S2). Then the slightly decreased n_{H2h} from one to another is mostly due to the inevitable loss of the catalyst occurring during the sample transfer process. Therefore, NC-7.5 is relatively stable for H_2 production under visible light in presence of sacrificial reagents. Note that a 7-repeated production of H_2 (14 h) was also conducted. After the photoreaction, the n_{H2h} value decreased by a factor of approximately 1.12 (Fig. S4).

3.3. Photocatalytic H_2O_2 production and decomposition

Reaction was carried out in an air-exposed aqueous solution without addition of sacrifices. Fig. 4A shows the results of H_2O_2 production on NC-x, measured under a 420 nm cut-off halogen lamp. As the irradiation time (t) increased, the concentration of H_2O_2 in aqueous phase ($[H_2O_2]$) increased. Among the samples, NC-3.0 was the most active. At 9 h, the $[H_2O_2]$ obtained for NC-3.0 was approximately 3 times higher than that measured for CdS (the insert in Fig. 4A). Control experiment with Ni_3S_4 alone showed a negligible production of H_2O_2. It is known that H_2O_2 once formed also decomposes in situ. Then the time profiles for H_2O_2 production fit to a kinetic equation of $[H_2O_2] = k_f/k_d\ [1 - \exp(-k_d t)]$, where k_f and k_d are the rate constants for H_2O_2 formation and decomposition, respectively [38], and the results are shown in Fig. 4B. As the Ni_3S_4 content increases, the k_f value increases initially, and then decreases. Meanwhile, the k_d value increases with x. These trends maintain unchanged if the solid surface area is taken into account (Fig. S5). The increased k_f with x is indicative of Ni_3S_4 promoting O_2 reduction on CdS. The decreased k_f with x is probably due to excess Ni_3S_4 reducing the number of photons reaching CdS. To confirm the Ni_3S_4 effect, experiment with 5 mM H_2O_2 was conducted, and the results are shown in Fig. 4C. In the dark, the amount of H_2O_2 adsorbed on Ni_3S_4 was much larger than that on CdS. Under visible light, the rate of H_2O_2 decomposition increased with the Ni_3S_4 loading on CdS. These observations indicate that Ni_3S_4 catalyzes the photocatalytic formation and decomposition of H_2O_2 on CdS, respectively.

To verify the origin of H_2O_2 production, several experiments were conducted (Fig. S6). In an air-exposed aqueous solution, the $[H_2O_2]$ produced at 3 h for CdS and NC-3.0 were 95.4 and 203 μM, respectively. In presence of 1 mM p-benzoquinone as superoxide radical scavenger, the corresponding $[H_2O_2]$ decreased to 16 and 8.2 μM, respectively. In the presence of 4% CH_3OH as hole scavenger, the corresponding $[H_2O_2]$ increased to 216 and 314 μM, respectively. In a N_2 bubbling aqueous solution, however, the corresponding $[H_2O_2]$ were only 16 and 8.7 μM, respectively. These observations indicate that most of H_2O_2 originates from O_2 reduction, instead of water oxidation. Then the average number of electrons (n_{ORR}) used for O_2 reduction was measured with a rotating disk electrode in 0.5 M $NaClO_4$ (see details in Fig. S7). The n_{ORR} for CdS, Ni_3S_4, and NC-3.0, were 1.08, 1.95, and 1.11, respectively. At given rotating speed and potential, the current was always $Ni_3S_4 >> $ NC-3.0 $>$ CdS. These observations indicate that Ni_3S_4 is more active than CdS for O_2 reduction in the dark, while the O_2 reduction occurring on CdS and Ni_3S_4 are two one-electron, and one two-electron processes, respectively.

3.4. Possible mechanism

In this work, the flat potential (E_{fb}) was measured in 0.5 M $NaClO_4$ through Mott-Schottky plots (Fig. S8). Both CdS and Ni_3S_4 were n-type semiconductors, and their E_{fb} were − 0.72 and − 0.39 V, respectively, against normal hydrogen electrode (NHE). Assuming that E_{fb} is equal to the conduction band edge potential (E_{cb}), then the valence band edge potentials (E_{vb}) for CdS and Ni_3S_4 are calculated to be 1.67 and 1.35 V (NHE), respectively. According to the band edge potentials, both the electron and hole transfer from CdS to Ni_3S_4 are feasible. If those processes occur at the same time, Ni_3S_4 is negative to CdS photocatalysis. In practice, Ni_3S_4 is positive to CdS photocatalysis, either for proton reduction to H_2, or for O_2 reduction to H_2O_2.

To elucidate the role of Ni_3S_4, an open circuit potential (OCP) test was conducted in a N_2 bubbling aqueous solution of 0.5 M $NaClO_4$, and the results are shown in Fig. 5A. On visible light illumination, the OCP immediately dropped down, and then reached a steady value. The former is due to fast generation of the photoelectrons on the electrode. The latter is due to equilibrium being achieved between the photoelectron generation and consumption. At the steady state, the OCP changes for CdS and NC-7.5 were 0.85 and 0.79 V, respectively. A bigger OCP change corresponds to a larger number of electrons remaining on the electrode. If CdS transfers its holes to NC-7.5, followed by water oxidation, the number of photoelectrons on the electrode should be increased. Therefore, there occurs only the electron transfer from CdS to Ni_3S_4, followed by proton reduction. After light was off, the OCP immediately raised up, and then slowly returned back to an original value. The former is due to fast recombination of the photoelectrons with the counterpart holes. The latter is indicative of the charge carriers still reacting with sorbates in the dark. In the latter process, the decay of OCP with time for NC-7.5 was slower than that for CdS. Through a kinetic curve fitting, the relevant rate constant (k_r) was estimated, which was 0.0048 s^{-1} for NC-7.5, and 0.0070 s^{-1} for CdS (Fig. S9). The smaller k_r of NC-7.5 than that of CdS is indicative of the electrons on NC-7.5 having a longer life time, as compared with those on CdS. This occurs if the "dark hole" oxidation of water on NC-7.5 is faster than that on CdS. It has been reported that Ni_3S_4 efficiently catalyzes the electrochemical

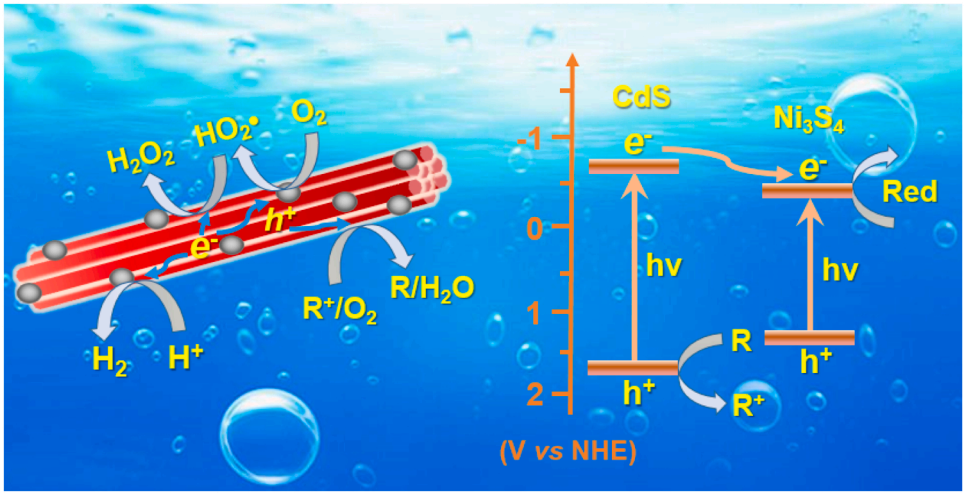

Scheme 1. A possible mechanism for the enhanced activity of Ni_3S_4/CdS.

oxidation of water.[32,34] Because of that, NC-7.5 exhibits a smaller k_r than CdS.

Then the electrochemical reduction of protons was checked, and the results are shown in Fig. 5B. As the potential swept toward a negative value, the cathode current increased, due to the increased proton reduction. At given potential, the dark current was Ni_3S_4 > NC-7.5 > CdS. Meanwhile, the corresponding onset potentials for the HER were − 0.499, − 0.445, and − 0.347 V vs. NHE, respectively (Fig. S9). Obviously, Ni_3S_4 is also a good catalyst for proton reduction, as in the cases for O_2 reduction and water oxidation, respectively. Because NC-7.5 has a smaller k_r than CdS, we speculate that the catalytic effect of Ni_3S_4 on water oxidation is larger than those on proton and O_2 reduction, respectively.

The positive effect of Ni_3S_4 on the charge transfer of CdS also coincides with the PL and EIS spectra, respectively (Fig. S10). On the excitation with 325 nm light, CdS had an emission peak at 525 nm (2.36 eV), well matching the band-to-band transition. After Ni_3S_4 loading, the emission intensity at 525 nm decreased by 198%. This is indicative of the charge transfer occurring from CdS to Ni_3S_4, followed by an increased reaction with sorbates. Through Nyquist plots, the charge transfer resistance at solid-liquid interface (R_{ct}) was measured. For CdS, NC-7.5, and Ni_3S_4, the R_{ct} values were 62.64, 46.87, and 35.89 Ω, respectively. These observations indicate that Ni_3S_4 efficiently mediates the electron transfer from CdS to species in solution.

In aqueous solution at pH 6.5, the H^+/H_2, O_2/H_2O_2, and O_2/H_2O couples have a redox potential of − 0.38, 0.32, and 0.85 V (NHE), respectively. Then both CdS and Ni_3S_4 are expected to be photoactive for all reactions ($2\ H^+ + 2e^- = H_2$, $O_2 + 2\ H^+ + 2e^- = H_2O_2$, $2\ H_2O + 4\ h^+ = O_2 + 4\ H^+$). In practice, Ni_3S_4 is poorly photoactive, due to its fast charge recombination. In principle, the electrons and holes of a semiconductor are generated and consumed in pairs. Any action that increases the electron transfer should promote the counterpart hole transfer and vice versa. Because Ni_3S_4 can capture the photoelectron of CdS, and catalyze proton and O_2 reduction, respectively, it shows a positive effect, either on proton reduction to H_2, or on O_2 reduction to H_2O_2. The above processes are presented in Scheme 1.

4. Conclusions

In this work, CdS nanowires have been modified with Ni_3S_4 nanoparticles. Under a 420 nm light, the samples containing 7.5% and 3.0% Ni_3S_4 are more active than others, for H_2 and H_2O_2 production, respectively. Behind that, the reaction rate decreases with the Ni_3S_4 content, due to excess Ni_3S_4 strongly absorbing light, and hence slowing down the CdS-photocatalyzed reaction. Under similar conditions, Ni_3S_4 is not photoactive, while a wavelength-dependent production of H_2 coincides with the absorption spectrum of CdS. With a film electrode, Ni_3S_4 is much more efficient than CdS in catalyzing proton and O_2 reduction, respectively. A study of the solid photoluminescence and band edge potentials suggests an interfacial charge transfer from CdS to Ni_3S_4, while a test of open circuit potential and charge resistance verifies an interfacial electron transfer from CdS to Ni_3S_4, followed by an increased reaction for proton reduction on Ni_3S_4 sites and for water oxidation on CdS sites. This work provides a simple route how to improve the CdS-based photocatalysis for the storage of solar energy.

CRediT authorship contribution statement

Wang Yaru: Conceptualization, Methodology, Software, Validation, Formal analysis, Investigation, Resources, Data curation, Writing – original draft, Writing – review & editing, Visualization. **Zhao Jianjun:** Investigation, Resources. **Hou Wenqing:** Resources. **Xu Yiming:** Writing – review & editing, Visualization, Supervision, Project administration, Funding acquisition.

Declaration of Competing Interest

The authors declare that they have no known competing financial interests or personal relationships that could have appeared to influence the work reported in this paper.

Acknowledgements

This work was supported by the Funds for Creative Research Group of NSFC (No. 21621005).

Notes

The authors declare no competing financial interest.

Appendix A. Supporting information

Supplementary data associated with this article can be found in the online version at doi:10.1016/j.apcatb.2022.121350.

References

[1] B. Lin, G. Yang, L. Wang, Stacking-layer-number dependence of water adsorption in 3D ordered close-packed g-C_3N_4 nanosphere arrays for photocatalytic hydrogen evolution, Angew. Chem. 58 (2019) 4587–4591.

[2] Y. Zheng, Z. Yu, H. Ou, A.M. Asiri, Y. Chen, X. Wang, Black phosphorus and polymeric carbon nitride heterostructure for photoinduced molecular oxygen activation, Adv. Funct. Mater. 28 (2018), 1705407.

[3] M.R. Hoffmann, S.T. Martin, W. Choi, D.W. Bahnemann, Environmental applications of semiconductor photocatalysis, Chem. Rev. 95 (1995) 69–96.

[4] T. Morikawa, S. Sato, K. Sekizawa, T. Arai, T.M. Suzuki, Molecular catalysts immobilized on semiconductor photosensitizers for proton reduction toward visible-light-driven overall water splitting, ChemSusChem 12 (2019) 1807–1824.

[5] L. Zheng, H. Su, J. Zhang, L.S. Walekar, H. Vafaei Molamahmood, B. Zhou, M. Long, Y.H. Hu, Highly selective photocatalytic production of H_2O_2 on sulfur and nitrogen co-doped graphene quantum dots tuned TiO_2, Appl. Catal. B 239 (2018) 475–484.

[6] Y. Isaka, Y. Kawase, Y. Kuwahara, K. Mori, H. Yamashita, Two-phase system utilizing hydrophobic metal-organic frameworks (MOFs) for photocatalytic synthesis of hydrogen peroxide, Angew. Chem. 58 (2019) 5402–5406.

[7] Z. Zhang, Y. Zhu, X. Chen, H. Zhang, J. Wang, A full-spectrum metal-free porphyrin supramolecular photocatalyst for dual functions of highly efficient hydrogen and oxygen evolution, Adv. Mater. 31 (2019), 1806626.

[8] S. Zhao, X. Zhao, Insights into the role of singlet oxygen in the photocatalytic hydrogen peroxide production over polyoxometalates-derived metal oxides incorporated into graphitic carbon nitride framework, Appl. Catal. B 250 (2019) 408–418.

[9] Q. Wu, Y. Liu, J. Cao, Y. Sun, F. Liao, Y. Liu, H. Huang, M. Shao, Z. Kang, A function-switchable Metal-free Photocatalyst for the efficient and selective production of hydrogen and hydrogen peroxide, J. Mater. Chem. A 8 (2020) 11773–11780.

[10] W.C. Huang, L.M. Lyu, Y.C. Yang, M.H. Huang, Synthesis of Cu_2O nanocrystals from cubic to rhombic dodecahedral structures and their comparative photocatalytic activity, J. Am. Chem. Soc. 134 (2012) 1261–1267.

[11] M. Barroso, A.J. Cowan, S.R. Pendlebury, M. Gratzel, D.R. Klug, J.R. Durrant, The role of cobalt phosphate in enhancing the photocatalytic activity of alpha-Fe_2O_3 toward water oxidation, J. Am. Chem. Soc. 133 (2011) 14868–14871.

[12] F. Wang, C. DiValentin, G. Pacchioni, Rational band gap engineering of WO_3 photocatalyst for visible light water splitting, ChemCatChem 4 (2012) 476–478.

[13] Y. Liu, Y. Deng, Z. Sun, J. Wei, G. Zheng, A.M. Asiri, S.B. Khan, M.M. Rahman, D. Zhao, Hierarchical Cu_2S microsponges constructed from nanosheets for efficient photocatalysis, Small 9 (2013) 2702–2708.

[14] W. Wu, G. Liu, Q. Xie, S. Liang, H. Zheng, R. Yuan, W. Su, L. Wu, A simple and highly efficient route for the preparation of p-phenylenediamine by reducing 4-nitroaniline over commercial cds visible light-driven photocatalyst in water, Green Chem. 14 (2012) 1705.

[15] J. Yu, Y. Yu, P. Zhou, W. Xiao, B. Cheng, Morphology-dependent photocatalytic H_2-production activity of CdS, Appl. Catal. B 156–157 (2014) 184–191.

[16] R. Shen, D. Ren, Y. Ding, Y. Guan, Y.H. Ng, P. Zhang, X. Li, Nanostructured CdS for efficient photocatalytic H_2 evolution: a review, Sci. China Mater. 63 (2020) 2153–2188.

[17] J. Bai, R. Shen, W. Chen, J. Xie, P. Zhang, Z. Jiang, X. Li, Enhanced photocatalytic H_2 evolution based on a $Ti_3C_2/Zn_{0.7}Cd_{0.3}S/Fe_2O_3$ Ohmic/S-scheme hybrid heterojunction with cascade 2D coupling interfaces, Chem. Eng. J. 429 (2022), 132587.

[18] Y. Zhou, Z. Tian, Z. Zhao, Q. Liu, J. Kou, X. Chen, J. Gao, S. Yan, Z. Zou, High-yield synthesis of ultrathin and uniform Bi_2WO_6 square nanoplates benefitting from photocatalytic reduction of CO_2 into renewable hydrocarbon fuel under visible light, ACS Appl. Mater. Interfaces 3 (2011) 3594–3601.

[19] H. Li, J. Shang, Z. Ai, L. Zhang, Efficient visible light nitrogen fixation with BiOBr nanosheets of oxygen vacancies on the exposed {001} facets, J. Am. Chem. Soc. 137 (2015) 6393–6399.

[20] Y. Lei, G. Wang, S. Song, W. Fan, M. Pang, J. Tang, H. Zhang, Room temperature, template-free synthesis of BiOI hierarchical structures: visible-light photocatalytic and electrochemical hydrogen storage properties, Dalton Trans. 39 (2010) 3273–3278.

[21] X. Wang, K. Maeda, X. Chen, K. Takanabe, K. Domen, Y. Hou, X. Fu, M. Antonietti, Polymer semiconductors for artificial photosynthesis: hydrogen evolution by mesoporous graphitic carbon nitride with visible light, J. Am. Chem. Soc. 131 (2009) 1680–1681.

[22] Y. Chen, L. Li, Q. Xu, T. Düren, J. Fan, D. Ma, Controllable synthesis of g-C_3N_4 INverse Opal Photocatalysts for Superior Hydrogen Evolution, Acta Phys. Chim. Sin. 0 (2020), 2009080-2009080.

[23] J.A. Nasir, Zu Rehman, S.N.A. Shah, A. Khan, I.S. Butler, C.R.A. Catlow, Recent developments and perspectives in CdS-based photocatalysts for water splitting, J. Mater. Chem. A 8 (2020) 20752–20780.

[24] A.V. Emeline, X. Zhang, M. Jin, T. Murakami, A. Fujishima, Application of a "Black Body" like reactor for measurements of quantum yields of photochemical reactions in heterogeneous systems, J. Phys. Chem. B 110 (2006) 7409–7413.

[25] X. Ning, G. Lu, Photocorrosion inhibition of CdS-based catalysts for photocatalytic overall water splitting, Nanoscale 12 (2020) 1213–1223.

[26] D. Ren, Z. Liang, Y.H. Ng, P. Zhang, Q. Xiang, X. Li, Strongly coupled ^2D–^2D nanojunctions between P-doped Ni_2S (Ni_2SP) cocatalysts and CdS nanosheets for efficient photocatalytic H_2 evolution, Chem. Eng. J. 390 (2020), 124496.

[27] C. Li, H. Wang, S.B. Naghadeh, J.Z. Zhang, P. Fang, Visible light driven hydrogen evolution by photocatalytic reforming of lignin and lactic acid using one-dimensional NiS/CdS nanostructures, Appl. Catal. B 227 (2018) 229–239.

[28] C. Zhang, B. Liu, X. Cheng, Z. Guo, T. Zhuang, Z. Lv, A CdS@NiS reinforced concrete structure derived from nickel foam for efficient visible-light H_2 production, Chem. Eng. J. 393 (2020), 124774.

[29] Z.H. Chen, C.C. Cheng, F.S. Xing, C.J. Huang, Strong interfacial coupling for NiS thin layer covered CdS nanorods with highly efficient photocatalytic hydrogen production, New J. Chem. 44 (2020) 19083–19090.

[30] Y. Yang, A.Q. Meng, X.L. Jiang, S.G. Meng, X.Z. Zheng, S.J. Zhang, X.L. Fu, S. F. Chen, Photocatalytic performance of NiS/CdS composite with multistage structure, ACS Appl. Energy Mater. 3 (2020) 7736–7745.

[31] X.Y. Liu, C.B. Bie, B.W. He, B.C. Zhu, L.Y. Zhang, B. Cheng, 0D/2D NiS/CdS nanocomposite heterojunction photocatalyst with enhanced photocatalytic H_2 evolution activity, Appl. Surf. Sci. 554 (2021).

[32] Y. Wang, Z.Q. Fang, Q.S. Dong, Y.Y. Chu, X.Y. Shi, M.X. Song, Z.M. Hao, Influence of the S:Ni ratio in raw materials on the Ni_xS_y electrocatalysts, Appl. Surf. Sci. 491 (2019) 590–594.

[33] B.H. Meekins, P.V. Kamat, Role of water oxidation catalyst IrO_2 in shuttling photogenerated holes across TiO_2 interface, J. Phys. Chem. Lett. 2 (2011) 2304–2310.

[34] K. Wan, J.S. Luo, C. Zhou, T. Zhang, J. Arbiol, X.H. Lu, B.W. Mao, X. Zhang, J. Fransaer, Hierarchical porous Ni_3S_4 with enriched high-valence ni sites as a robust electrocatalyst for efficient oxygen evolution reaction, Adv. Funct. Mater. 29 (2019).

[35] M. Qureshi, K. Takanabe, Insights on measuring and reporting heterogeneous photocatalysis: efficiency definitions and setup examples, Chem. Mater. 29 (2016) 158–167.

[36] H. Bader, V. Sturzenegger, J. Hoigné, Photometric method for the determination of low concentrations of hydrogen peroxide by the peroxidase catalyzed oxidation of N,N-diethyl-p-phenylenediamine (DPD), Water Res. 22 (1988) 1109–1115.

[37] D.L. Legrand, H.W. Nesbitt, G.M. Bancroft, X-ray photoelectron spectroscopic study of a pristine millerite (NiS) surface and the effect of air and water oxidation, Am. Mineral. 83 (1998) 1256–1265.

[38] B.O. Burek, D.W. Bahnemann, J.Z. Bloh, Modeling and optimization of the photocatalytic reduction of molecular oxygen to hydrogen peroxide over titanium dioxide, ACS Catal. 9 (2019) 25–37.